Journal of Magnetic Resonance 214 (2012) 273–280

Contents lists available at SciVerse ScienceDirect

Journal of Magnetic Resonance

journal homepage: www.elsevier.com/locate/jmr

Measuring T_2 and T_1, and imaging T_2 without spin echoes

G. Wang [a,b,1], A.M. El-Sharkawy [a,1], W.A. Edelstein [a], M. Schär [a,c], P.A. Bottomley [a,b,*]

[a] Department of Radiology and Radiological Science, Johns Hopkins University, Baltimore, MD, USA
[b] Department of Electrical and Computer Engineering, Johns Hopkins University, Baltimore, MD, USA
[c] Philips Healthcare, Cleveland, OH, USA

ARTICLE INFO

Article history:
Received 20 September 2011
Revised 18 November 2011
Available online 7 December 2011

Keywords:
Spin–spin relaxation
Measurement
Adiabatic pulses
Spin–lattice relaxation
MRI
T_1
T_2

ABSTRACT

During adiabatic excitation, the nuclear magnetization in the transverse plane is subject to T_2 (spin–spin) relaxation, depending on the pulse length τ. Here, this property is exploited in a method of measuring T_2 using the ratio of NMR signals acquired with short and long-duration self-refocusing adiabatic pulses, without spin-echoes. This Dual-τ method is implemented with B_1-insensitive rotation (BIR-4) pulses. It is validated theoretically with Bloch equation simulations independent of flip-angle, and experimentally in phantoms. Dual-τ T_2 measurements are most accurate at short T_2 where results agree with standard spin-echo measures to within 10% for $T_2 \leqslant 100$ ms. Dual-τ MRI performed with a long 0° BIR-4 pre-pulse provides quantitative T_2 imaging of phantoms and the human foot while preserving desired contrast and functional properties of the rest of the MRI sequence. A single 0° BIR-4 pre-pulse can provide T_2 contrast-weighted MRI and serve as a "T_2-prep" sequence with a lower B_1 requirement than prior approaches. Finally, a Tri-τ experiment is introduced in which both τ and flip-angle are varied, enabling measurement of T_2, T_1 and signal intensity in just three acquisitions if flip-angles are well-characterized. These new methods can potentially save time and simplify relaxation measurements and/or contrast-weighted NMR and MRI.

1. Introduction

The term *adiabatic* as applied to NMR excitation pulses refers to frequency and/or amplitude modulated pulses whose effective B_1-field in the frame-of-reference rotating at the Larmor frequency change sufficiently slowly such that the nuclear magnetization **M** is able to follow it without inducing transitions[1,2]. Adiabatic pulses are highly-valued for their insensitivity to RF and static magnetic field (B_0) inhomogeneity over ranges determined by the pulse duration τ, flip-angle θ, and transverse RF field (B_1) amplitude and frequency sweep [3]. The duration of the pulses is supposed to be shorter than any relaxation processes–whence the term, *fast passage*.

In the classic experiment, the frequency was swept linearly through resonance [1,2]. Nowadays, adiabatic full-passage (AFP; $\theta = 180°$) and half passage (AHP; $\theta = 90°$) pulses with $B_1(t)$ amplitude/frequency-sweeps that vary as sin/cos, tan/tanh and sech/tanh, offer far superior B_1-performance [2–5]. The BIR-4 (B_1-insensitive rotation) pulse, which combines four AHP segments, has further extended adiabaticity to flip-angles that can be arbitrarily set anywhere in the range $|\theta| \leqslant 180°$ [6]. The BIR-4 flip-angle is set by means of two phase-jumps between the segments, which can be phase-cycled to improve accuracy [7].

All of these adiabatic pulses, and especially the BIR-4 pulses, are intrinsically longer than conventional hard pulses. To the extent that the magnetization **M** evolves in the transverse plane during the pulse, it is subject to transverse T_2 (spin–spin) decay, even when the pulses are self-refocusing [3,8,9]. This dependence is potentially exploitable for measuring T_2 or for enhancing T_2 contrast. To date, except for the use of spectral linewidths, T_2 has been measured with NMR spin-echoes (SEs). The most accurate T_2 measurements are derived from the Carr–Purcell–Meiboom–Gill (CPMG) technique [10]. SEs are routinely used to provide critically important T_2-dependent contrast and T_2 measurements in clinical diagnostic magnetic resonance imaging (MRI) [11].

Here we present a new approach for measuring T_2 in NMR and MRI, and for providing T_2 contrast in MRI, that does not use SEs. Instead, the T_2 dependence of adiabatic pulses is harnessed to measure T_2 by repeating the NMR or MRI acquisition sequence using one or more different adiabatic pulse lengths τ. We introduce the Dual-τ method, which provides a T_2 measurement from the ratio of NMR signals acquired with short- and long-duration adiabatic pulses. This is analogous to the *dual-angle* method for measuring the T_1 (spin–lattice) relaxation time from the ratio of signals acquired with two BIR-4 pulse flip-angles. Indeed, addition of a third acquisition permits the measurement of *both* T_2 and T_1 using a

* Corresponding author. Address: Division of MR Research, Department of Radiology, Johns Hopkins School of Medicine, 600 N. Wolf Street, Park 311, Baltimore, MD 21287, USA.
E-mail address: bottoml@mri.jhu.edu (P.A. Bottomley).
[1] These authors contributed equally to the work.

1090-7807/$ - see front matter © 2011 Elsevier Inc. All rights reserved.
doi:10.1016/j.jmr.2011.11.016

combination of different pulse lengths and flip-angles in the Tri-τ method, also introduced herein. Both the Dual-τ and the Tri-τ methods are implemented with self-refocusing BIR-4 pulses and validated by Bloch equation simulations, and by experimental studies of phantoms whose T_2s and T_1s are measured by standard CPMG, SE and partial saturation (PS) methods. The simulations provide a look-up table or curve which is used to convert measured signal ratios into T_2 values. T_1 is determined from a formula analogous to that used for the *dual-angle* method [12].

Because adiabatic pulses are generally unsuitable for spatially-selective excitation in MRI, implementation of the Dual-τ method in imaging is most easily accomplished by addition of a 0° BIR-4 pre-pulse to the conventional MRI sequence. Since a 0° pulse does not otherwise affect the nuclear spin dynamics, other desirable MRI contrast and functional properties built into the sequence that follows the pre-pulse can be preserved. A single 0° BIR-4 pre-pulse of length τ can provide T_2-contrast or T_2-weighted MRI, as well as "T_2-prep" (T_2-preparation) MRI with a lower B_1 threshold than T_2-prep sequences employing AHP and AFP pulses [13]. Quantitative Dual-τ T_2 imaging can be performed by applying MRI sequences with and without the 0° τ pre-pulse. The Dual-τ T_2 MRI method is validated with studies of phantoms and the human foot by comparison with standard CPMG methods.

2. Theory

2.1. Dual-τ T_2 measurements

The longitudinal and transverse magnetization with magnitudes denoted M_z and M_{xy}, are affected by both T_1 and T_2 relaxation following a long adiabatic pulse [9]. At the end of an adiabatic pulse with flip angle θ (time 0^+), $M_z(0^+) = \cos\theta M_z(0^-)E_p^z$ and $M_{xy}(0^+) = \sin\theta M_{xy}(0^-)E_p^{xy}$, as compared to the start of the pulse (time 0^-). Here E_p^z and E_p^{xy} are longitudinal and transverse attenuation factors, which are functions of τ, T_2, B_1 and the maximum frequency sweep, f_{max}, of the pulse, but not T_1, provided that $\tau \ll T_1$. After self-refocusing at the end of the adiabatic pulse, the T_2 decay can be written as $E_p^{xy} = e^{-g\tau/T_2}$, where g is a parameter reflecting the fraction of time spent by the magnetization in the transverse plane during the pulse.

If the residual transverse magnetization prior to time 0^- is crushed [14], the steady-state magnetization after a sequence of adiabatic pulses applied at a repetition period TR comparable to T_1 is [9]:

$$M_z(0^+) = M_0\frac{(1-E_1)\cos\theta E_p^z}{1-\cos\theta E_p^z E_1};\quad M_{xy}(0^+) = M_0\frac{(1-E_1)\sin\theta E_p^{xy}}{1-\cos\theta E_p^z E_1} \tag{1}$$

where $E_1 = e^{-TR/T_1}$ and M_0 is the equilibrium nuclear magnetization. If θ = 90°, the application of two such sequences with the same TR but two different pulse durations τ_1 and τ_2, will produce steady-state signals

$$M_{xy}(\tau=\tau_1) = M_0(1-E_1)E_{p1}^{xy} \text{ and } M_{xy}(\tau=\tau_2) = M_0(1-E_1)E_{p2}^{xy}.$$

The ratio of these signals is:

$$R = \frac{M_{xy}(\tau=\tau_1)}{M_{xy}(\tau=\tau_2)} = \frac{M_0(1-E_1)E_{p1}^{xy}}{M_0(1-E_1)E_{p2}^{xy}} = \frac{E_{p1}^{xy}}{E_{p2}^{xy}} = \frac{E_{p1}}{E_{p2}} \tag{2}$$

where E_{p1} and E_{p2} are the attenuation factors for the two pulses. Here we have set $E_p = E_p^z = E_p^{xy}$ based on numerical analyses of the Bloch equations with BIR-4 pulses of duration τ < 40 ms, that shows that the attenuation of the magnetization, E_P = |M|/M_0, is independent of flip-angle at least up to 90° for $200 \leqslant T_1 \leqslant 1000$ ms and $5 \leqslant T_2 \leqslant 200$ ms. Eq. (2) shows that R is just a function of T_2 which can be derived numerically from the known B_1 and f_{max}.

If θ = 0°, as in the case of a sequence comprised of a 0° BIR-4 pre-pulse followed by a short 90° readout pulse, M_{xy} is attenuated in a similar fashion by E_p^z. The signal following the read-out pulse if two different-duration 0° BIR-4 pre-pulses are used is $M_{xy}(\tau=\tau_1) = M_0(1-E_1)E_{p1}^z$ and $M_{xy}(\tau=\tau_2) = M_0(1-E_1)E_{p2}^z$. Their ratio is $R = \frac{E_{p1}^z}{E_{p2}^z} = \frac{E_{p1}}{E_{p2}}$, the same as in Eq. (2).

2.2. Tri-τ T_2 and T_1 measurements

When TR is short, the Dual-τ method is limited to choices of θ = 90° (or a θ = 0° BIR-4 pulse followed by a 90°) to cancel troublesome terms in Eq. (1). Incomplete cancellation can occur due to pulse imperfections, incomplete dephasing of residual transverse magnetization, and/or deviations in E_p as TR approaches T_2. Achieving perfect 90° pulses is often problematic for *in vivo* applications such as MRI where the pulses are slice-selective and the RF fields are seldom uniform across the slice. While increasing TR can alleviate this problem, long TRs generally reduce the signal-to-noise (SNR) ratio per unit time and increase the scan time. These limitations are overcome by adding a third acquisition to accommodate both θ < 90° pulses and short TRs. Importantly, the additional acquisition can permit a simultaneous determination of both T_1 and T_2.

We call this the Tri-τ method, in which: (1) a first signal S_1 is acquired with a conventional short α RF excitation pulse without adiabatic excitation; (2) a second signal S_2 is excited by a β adiabatic pulse of duration τ_2; and (3) a third signal S_3 is excited by a β adiabatic of length $\tau_3 = 2\tau_2$. The three steady-state signals are:

$$S_1 = \frac{(1-E_1)\sin\alpha}{(1-E_1\cos\alpha)}M_0,\quad S_2 = \frac{(1-E_1)E_{p2}\sin\beta}{(1-E_1E_{p2}\cos\beta)}M_0 \text{ and}$$
$$S_3 = \frac{(1-E_1)E_{p3}\sin\beta}{(1-E_1E_{p3}\cos\beta)}M_0 \tag{3}$$

Using the same B_1 and f_{max} for both adiabatic pulses yields $E_p = e^{-g\tau/T_2}$, $E_{p3} = E_{p2}^2$, and Eq. (3) simplifies to a quadratic:

$$aE_{p2}^2 + bE_{p2} + c = 0, \tag{4}$$

where $a = S_1\sin\beta\cos\beta\sin\alpha(S_3 - S_2)$, $b = S_1S_2\sin\alpha\cos\alpha\sin\beta - S_2S_3\sin^2\alpha\cos\beta$, and $c = S_2S_3\sin^2\alpha\cos\beta - S_1S_3\sin\alpha\cos\alpha\sin\beta$.

Choosing the root of Eq. (4) that falls in the interval (0,1) yields the T_2 attenuation factor

$$E_{p2} = \frac{-b \pm \sqrt{b^2-4ac}}{2a}. \tag{5}$$

Substitution of Eq. (5) into Eq. (3) yields the T_1 exponential decay factor:

$$E_1 = \frac{S_2\sin\alpha - S_1\sin\beta E_{p2}}{(S_2\sin\alpha\cos\beta - S_1\cos\alpha\sin\beta)E_{p2}} \text{ or}$$
$$E_1 = \frac{S_3\sin\alpha - S_1\sin\beta E_{p3}}{(S_3\sin\alpha\cos\beta - S_1\cos\alpha\sin\beta)E_{p3}} \tag{6}$$

This is basically the *dual-angle* equation [12] with an E_{p2}-attenuation correction. Thus, from E_{p2} and E_1:

$$T_2 = -\frac{g\cdot\tau_2}{\ln(E_{p2})} \text{ and } T_1 = -\frac{TR}{\ln(E_1)}. \tag{7}$$

3. Material and methods

3.1. Numerical simulations

Simulations of the Bloch equations were performed using Matlab (Mathworks, Natick, MA)[15]. The evolution of magnetization

was simulated for proton (^{1}H) relaxation at 3 T over the range $20 \leqslant T_2 \leqslant 200$ ms and $0.1\text{ s} \leqslant T_1 \leqslant 1$ s for BIR-4 pulses with $B_1 = 20$ μT, $f_{max} = 15$ kHz, and offset frequencies of ±300 Hz, as used in experiments. Pulses were defined at 5 μs intervals with lengths varying from $1 \leqslant \tau \leqslant 40$ ms, a practical range given limitations in RF pulse power and power deposition. Adiabatic pulse flip-angles were varied from $0 \leqslant \theta \leqslant 90°$. The simulations were used to derive the attenuation factors, E_p^z and E_p^{xy} after long BIR-4 pulses, decay parameter g, and the corresponding signal ratio R, as a function of T_2, T_1, τ, and θ in the Dual-τ experiment.

Monte Carlo simulations were performed to evaluate the sensitivity of Dual-τ and Tri-τ measurements, to noise. The standard deviation (SD) of the noise was set at 2% of the signal strength (SNR = 50) elicited by each pulse. The signals, their ratio R for the Dual-τ T_2 experiment, and the solutions to Eq. (7) for the Tri-τ experiment, were determined for 1000 simulations as a function of T_2 up to 80 ms in the Dual-τ and Tri-τ experiments, and $0.1\text{ s} \leqslant T_1 \leqslant 1$ s for the Tri-τ experiment. Note that T_2 measured by the Dual-τ experiment is unaffected by TR for perfect $\theta = 90°$ pulses.

The utility of a single 0° BIR-4 pre-pulse for providing T_2-contrast, T_2-weighting or T_2-prep MRI was simulated for BIR-4 pulses with $\tau \leqslant 45$ ms, $B_1 \leqslant 100$ μT and offset frequencies ⩽±800 Hz. Results were compared with the AHP/AFP T_2-prep sequence of Ref. [13].

3.2. Phantom preparation

Twelve phantoms with tissue-comparable relaxation times were prepared with agarose (Type 1-A CAS 9012-36-3: Sigma Chemical, St. Louis, MO, USA) and $CuSO_4$ (CAS 7758-99-8: Acros organics, Geel, Belgium) in de-ionized distilled water. Both agarose and $CuSO_4$ shorten the T_1 and T_2 of pure water. However, agarose decreases T_2 more effectively than $CuSO_4$, which more strongly affects T_1. The concentrations of $CuSO_4$ and agarose were adjusted from 0.2 to 1.6 g/l and 10 to 110 g/l respectively, to provide phantoms with $10\text{ ms} < T_2 < 130$ ms, and $0.15\text{ s} < T_1 < 1.0$ s [16]. The ingredients were mixed in a beaker and heated in a microwave oven to dissolve the agarose without introducing too many bubbles. The hot solutions were then sealed in 25 mm inner diameter (ID) plastic tubes and allowed to cool and gel. Tubes were filled to about 9 or 4 cm for the Dual-τ and Tri-τ experiments respectively.

3.3. NMR measurements

All NMR and MRI measurements were done on a 3 T Achieva MRI scanner (Philips Healthcare, Best, The Netherlands) using the standard transmit/receive birdcage head coil (maximum $B_1 = 20$ μT). The gel phantoms were set in a plastic foam panel in the center of the coil with long axes parallel to the z-axis. To facilitate T_1 and T_2 measurements, NMR data were acquired with one-dimensional chemical shift imaging (1D CSI, 5 mm resolution; acquisitions per frame, NEX = 1) from five aligned phantoms at a time. In all measurements involving BIR-4 pulses, the flip angles were calibrated at the pulse lengths being tested by determining the phase-jump offset at which a 0° BIR-4 pulse produced near-zero signal (<2%) [7], and then verifying that a 90° BIR-4 pulse with the same offset yielded maximum fully-relaxed signal. Dual-τ T_2 was measured with two 90° BIR-4 pulses of lengths $\tau_1 = 5$ ms ($f_{max} = 12$ kHz) and $\tau_2 = 35$ ms ($f_{max} = 15$ kHz), the shortest TE (1.8 ms) and TR = 4 s.

Reference T_2 and T_1 relaxation times were measured at 3 T using standard SE and PS NMR methods, respectively. Individual SE data was obtained using 1D CSI with eight different echo times (TE = 14, 30, 50, 75, 100, 150, 200, 300 ms). TR was set to 4.0 s to allow for complete signal recovery. T_1 was measured using PS sequences with TR = 0.25, 0.5, 1, and 3 s. Because relaxation times can change slowly over time, these measurements were repeated whenever a dual- or Tri-τ study was done. The effect of offset frequency on T_2 accuracy was tested separately in CSI experiments on five of the short phantoms with T_2s of 30–60 ms at offset frequencies of ⩽300 Hz.

The CSI experiments yielded approximately five slices in the CSI direction from each phantom. The free induction decays (FID) acquired from the three middle slices in each phantom were fitted using jMRUI software (available from www.mrui.uab.es)[17] to determine the peak areas. These values were used to determine the signal ratio at the two τ values. Dual-τ T_2 was then determined from a look-up curve generated by the numerical analysis (see Section 4). Reference T_1 and T_2 measurements obtained by conventional SE and PS methods were determined from the same three slices by fitting the data sets to $\{w\exp(-TE/T_2)\}$ and $\{u - v\exp(-TR/T_1)\}$ with u, v and w constants. Mean reference relaxation times from the phantoms used in the Dual-τ studies are listed in Table 1.

The Tri-τ method was also validated in 1DCSI studies of 12×1.3 cm ID and 4×2.5 cm ID phantoms with $169 \leqslant T_1 \leqslant 890$ ms and $31 \leqslant T_2 \leqslant 129$ ms. We used $\tau_3 = 2\tau_2 = 20$ ms, and TR = 300 ms for all experiments. Shorter TRs were limited by RF power restrictions. S_1 was acquired with a (non-adiabatic) 75 μs hard pulse nominally set to $\alpha = 15°$. The flip-angle was 14° for the short phantoms as determined from B_1 field profiles measured separately, and 13.5° for the long phantoms. The β-pulse used to acquire S_2 and S_3 was a 60° BIR-4 pulse. The choice of the nominal $\alpha = 15°$ and $\beta = 60°$ pair for the Tri-τ experiments was based on the *dual-angle* T_1 method [12].

3.4. MRI measurements

The BIR-4 pulse is unsuited to spatial localization. Thus for MRI applications, either multi-dimensional phase-encoding must be used (with generally unpalatable scan times), or the BIR-4 pulse must be applied in conjunction with an additional spatial localization pulse. We adopt the latter approach by adding a 0° BIR-4 pulse before the slice-selective pulse in a standard gradient-echo (FFE) MRI pulse sequence, as simulated.

Dual-τ MRI was performed on the phantom set with a two-dimensional (2D) FFE MRI sequence and 0° BIR-4 pulses with the same τ, f_{max} and B_1 used in the NMR experiments (acquisition matrix, 152×154; field-of-view, FOV = $97 \times 10 \times 230$ mm^3; slice thickness = 10 mm; TR = 2 s; minimum TE = 2.5 ms). The delay between the BIR-4 and (1 ms) slice-selective pulses was 1.5 ms. Because the excitation pulse and inter-pulse delay are unchanged in this Dual-τ MRI experiment, the same curve from the numerical analysis was used to obtain T_2. The sequence timing diagram is shown in Fig. 1. Reference T_2 values from conventional MRI were obtained from the phantoms using a three-dimensional (3D) CPMG sequence (32 echoes, TE step = 7.21 ms, TR = 461 ms, 2.5 ms excitation pulse 1.5 ms after the BIR-4 pulse). T_2 was measured in images by determining the ratio R on a pixel-by-pixel basis for the Dual-τ method, and by fitting the SE pixels to an exponential to obtain reference T_2 images. Pixel-average T_2 values within each phantom are reported (means ± standard deviation, SD). The consistency of T_2 measured by SE 1D CSI and CPMG MRI was verified with measurements on five additional phantoms with $T_2 = 30$–60 ms.

Human studies for this project were approved by the Johns Hopkins Institutional Review Board. The foot was chosen based on the expected short T_2s of muscle and cartilage [18], for which analysis showed the Dual-τ method to be well-suited. A healthy volunteer was positioned supine with the foot in the head coil, and Dual-τ T_2 MRI performed using two acquisitions of a coronal 3D FFE sequence, one employing a 0° BIR-4 pre-pulse (matrix size,

Table 1
Phantoms with their relaxation times for the Dual-τ T_2 NMR and MRI studies.

Dual-τ phantoms												
T_2 (ms)	110	97	65	65	52	44	35	28	18	13	106	67
T_1 (ms)	818	837	770	740	691	702	665	635	567	582	825	–
Tri-τ phantoms												
T_2 (ms)	101	30	49	33	129	30	32	31.5	38.1	37.6	59.2	57.7
T_1 (ms)	890	441	219	379	558	448	375	698	315	389	248	169

T_2 was measured by a 32-point CPMG method (TE stepped by 7.21 ms). T_1 was measured by PS ($0.1\text{ s} \leqslant \text{TR} \leqslant 1.5\text{ s}$). The signal within each phantom was first averaged then fit to an exponential relaxation curve.

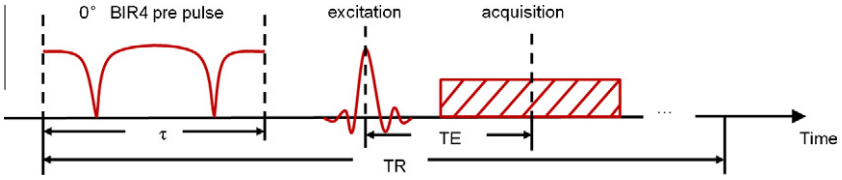

Fig. 1. Timing diagram of a sequence employing one of 0° BIR-4 pre-pulses for the Dual-τ MRI method. In MRI experiments TE was set to a minimum (4.8 ms), TR at 2 s, and the gap between the pre- and excitation-pulses was ~1.5 ms.

112×112; slice thickness = 6 mm; FOV = $42 \times 100 \times 100\text{ mm}^3$, TR = 2 s, TE = 4.1 ms = minimum). Reference T_2 MRI of the foot was performed with the 32-echo CPMG sequence (same matrix, slice thickness and FOV as for Dual-τ FFE; TE step = 5.39 ms; TR = 625 ms). T_2 images and average T_2 values were calculated the same way as in the phantom studies.

4. Results

4.1. Numerical analysis

The attenuation factor, E_p as a function of T_2 is plotted in Fig. 2 for four BIR-4 pulses of duration 5–35 ms. The curves all fit accurately to the exponential $E_p(T_2) = \exp\left(-0.81\frac{\tau}{T_2}\right)$. In this case, $g = 0.81$. A side-effect of this result is that the T_2 attenuation from a single long duration τ_2 adiabatic pulse is the same as that resulting from concatenation of n short τ_1 pulses of the same total duration τ_2, except for an approximately n-fold increase in B_1 to achieve adiabaticity. The result in Fig. 2 is also independent of flip-angle for $0° \leqslant \theta \leqslant 90°$ and for long TR, reflecting the fact that the BIR-4 flip-angle is set by two opposite phase-jumps of duration much less than τ, T_2 and T_1. In the adiabatic region wherein θ is independent of B_1, g is relatively insensitive to f_{max}, for example, varying from 0.79 to 0.81 for $12\text{ kHz} \leqslant f_{max} \leqslant 15\text{ kHz}$ and $B_1 = 20\ \mu\text{T}$.

The sensitivity and accuracy of the Dual-τ T_2 experiment are improved by selecting BIR-4 pulses with very different pulse lengths, notwithstanding RF power constraints. Pulses shorter than 5 ms have little attenuation but are limited by peak pulse power. Long pulses are limited by the RF power amplifier's ability to sustain the pulse, as well as by the spectral bandwidth of the sample. The ratio of the signals from the $\tau_1 = 5$ ms and $\tau_2 = 35$ ms pulses is plotted in Fig. 3a. The curve is fit by $R(T_2) = \exp(-24.3/T_2)$ independent of θ. Sensitivity is maximum over the steepest (short-T_2) region of the curve, with the $\tau_1/\tau_2 = 5/35$ ms pair providing reasonable T_2 resolution up to 70 or 80 ms. Thus, T_2 can be read from Fig. 3(a) using the measured signal ratio. The variation in T_2 determined from the ratio curve is plotted as a function of T_1 in Fig. 3(b). The result varies by <1% for $0.6\text{ s} \leqslant T_1 \leqslant 1.0\text{ s}$, and <6% for $0.2\text{ s} \leqslant T_1 \leqslant 1.0\text{ s}$, but begins to introduce errors as T_2 approaches T_1. The results of the analysis of the affect of offset frequencies of up to ±300 Hz, show that T_2 varies by <6.5% for $30\text{ ms} \leqslant T_2 \leqslant 130\text{ ms}$, TR = T_1 = 1 s and $B_1 = 20\ \mu\text{T}$.

The results of the Monte Carlo simulations are exemplified in Fig. 4. For the Dual-τ T_2 experiment performed with $\tau_1/\tau_2 = 5/35$ ms pulses and signals with 2% SD, the errors are essentially independent of TR for $0.1\text{ s} \leqslant \text{TR} \leqslant 1.0\text{ s}$. Over this range, the mean error in T_2 is less than 6% ± 9% (SD) of T_2 for $T_2 \leqslant 80$ ms and $0.3\text{ s} \leqslant T_1 \leqslant 1\text{ s}$ (Fig. 4a). On the other hand, the simulated Tri-τ experiment with $\tau_3 = 2\tau_2 = 20$ ms is less accurate on average, with a mean error varying from -13% to +6% of T_2 (with up to ±30%SD scatter) for $T_2 \leqslant 80$ ms over the ranges $0.1\text{ s} \leqslant \text{TR} \leqslant 1.0\text{ s}$ and $0.1 \leqslant T_1 \leqslant 1\text{ s}$ (Fig. 4b). When τ_3 is set to 35 ms – the same as τ_2 in the Dual-τ experiment – the mean error decreases to <13% ± 17% (SD) of T_2 for the same T_1s and TRs (e.g., Fig. 4c).

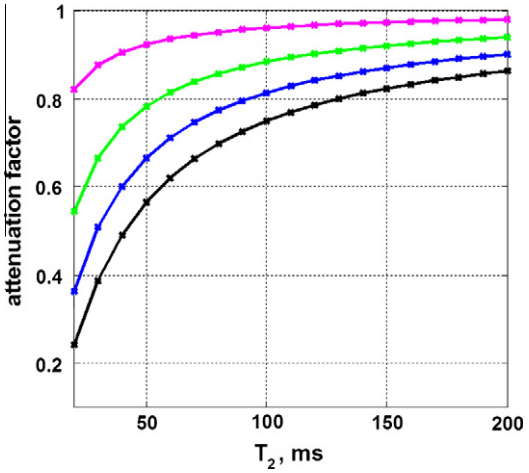

Fig. 2. Numerical simulation of the attenuation factor $E_P = |M|/M_0$ of the magnetization after a BIR-4 pulse of duration 5 ms (magenta), 15 ms (green), 25 ms (blue) and 35 ms (black), as a function of T_2 from 20 to 200 ms ($T_1 = 1$ s, TR = ∞ for complete longitudinal relaxation) with $f_{max} = 15$ kHz and $B_1 = 20\ \mu$T. The curves are exponential fits to the numerically-determined points (stars) from which $g = 0.81$ and valid for θ up to 90°. (For interpretation of the references to colour in this figure legend, the reader is referred to the web version of this article.)

The accuracy of T_1 in the Monte Carlo simulations of the Tri-τ experiment is better than 1% of T_1 with a 9–15%(SD) scatter, essentially independent of pulse length for $0.3 \leqslant T_1 \leqslant 1\text{ s}$ and $30 \leqslant T_2 \leqslant 130$ ms, as shown in Fig. 4d for TR = 0.3 s. At shorter T_1s (<TR), the scatter in T_1 increases as the long TR becomes suboptimal for measuring T_1 [8]. In this case, reducing TR to 0.1 s, reduces the scatter back to 9–15% of T_1 for $0.1 \leqslant T_1 \leqslant 1.0\text{ s}$.

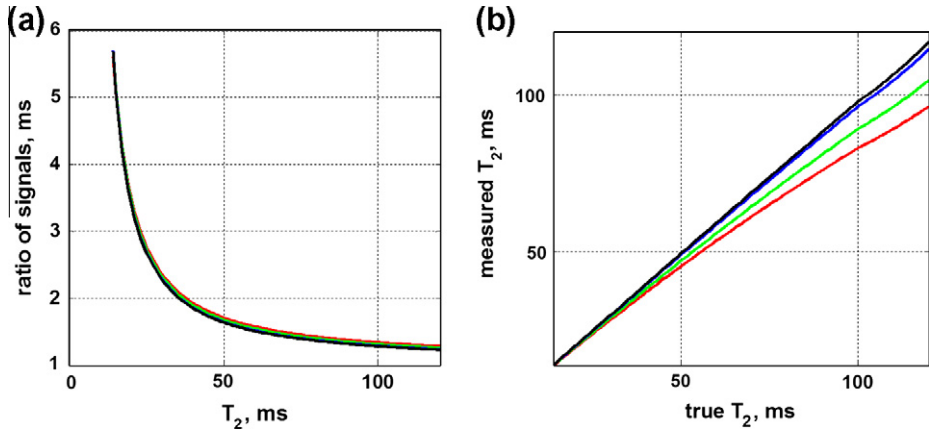

Fig. 3. (a) Computed ratio R of two signals acquired with adiabatic pulses of length τ_1 = 5 ms with g = 0.79 for f_{max} = 12 kHz and τ_2 = 35 ms with g = 0.81 for f_{max} = 15 kHz, as a function of T_2 for T_1s of 0.12–1 s. The curve has the form $R(T_2) = \exp\left(\frac{-0.81\times35+0.79\times5}{T_2}\right) = \exp\left(\frac{-24.4}{T_2}\right)$. (b) Dual-$\tau$ T_2 determined from part (a) as a function of T_1 (red, T_1 = 0.12 s; green, T_1 = 0.2 s; blue, T_1 = 0.6 s; black, T_1 = 1.0 s). The result is independent of TR. (For interpretation of the references to colour in this figure legend, the reader is referred to the web version of this article.)

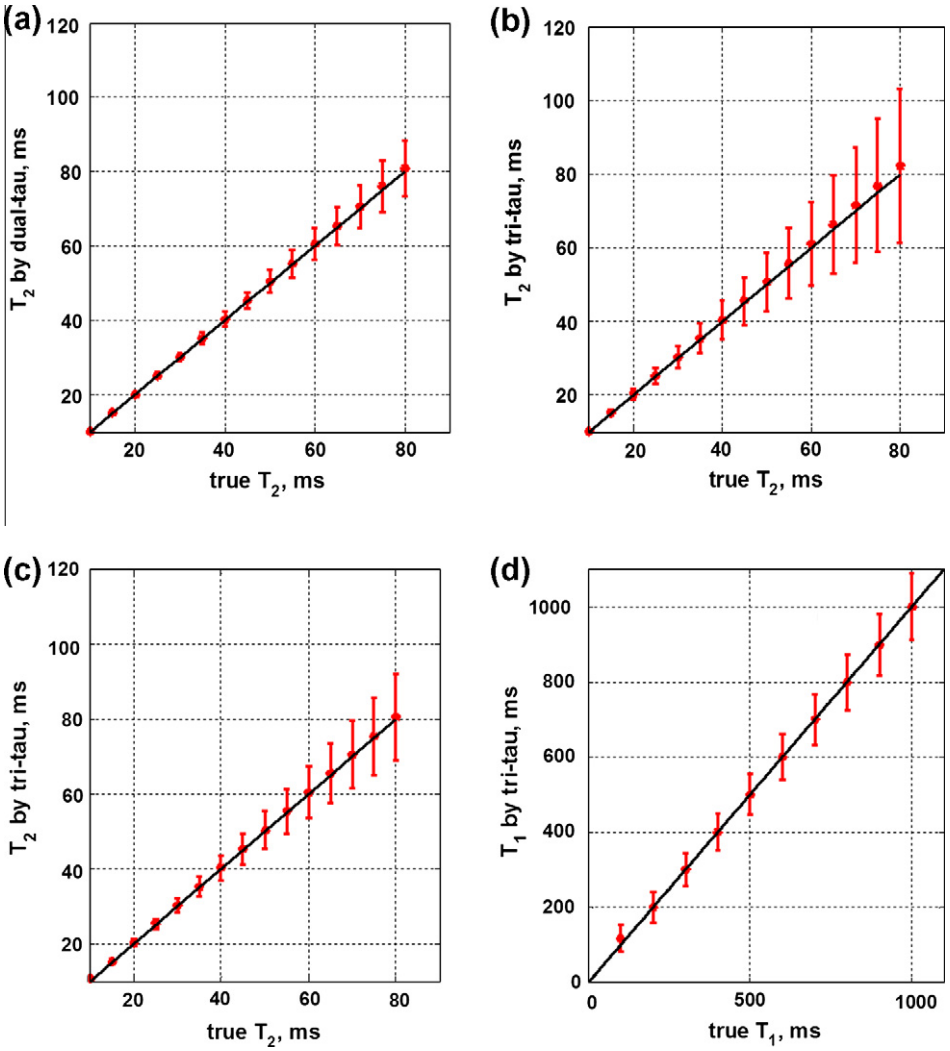

Fig. 4. Monte Carlo simulations of the error in (a) Dual-τ T_2 with τ_1 = 5 ms and τ_2 = 35 ms; (b) Tri-τ T_2 with $\tau_3 = 2\tau_2$ = 20 ms; and (c) with $\tau_3 = 2\tau_2$ = 35 ms; and (d) Tri-τ T_1 with $\tau_3 = 2\tau_2$ = 20 ms, T_2 = 40 ms, and TR = 300 ms. Points are means ± SD for a 2% root-mean-square noise in each signal measurement (SNR = 50) from 1000 runs with T_1 = 1 s. The mean and SD of the T_1 measured by a Tri-τ experiment with $\tau_3 = 2\tau_2$ = 35 ms differs from (d) by less than 1%.

The performance of a 45 ms 0° BIR-4 pre-pulse for T_2-prep MRI is shown in Fig. 5 for a sample with T_2 = 55 ms. The B_1 threshold is approximately 5 μT, and the pulse attenuates M_z by $\exp(-0.81 \times 45/T_2) \approx 0.5$ over a broad range of B_1 and offset frequencies.

4.2. Experiments

Results from the ^{1}H 1D CSI Dual-τ validation experiments on the 10 phantoms are plotted in Fig. 6. The T_1 of these phantoms was 0.6–0.8 s (Table 1). The T_2s were determined from Fig. 3. Below T_2 = 70 ms, Dual-τ T_2 values differ from SE values by ⩽3%. The accuracy of T_2 varied ⩽7% for offset frequencies ⩽300 Hz compared to T_2 measured on resonance, consistent with the simulations.

Dual-τ T_2-weighted and T_2-image results from the phantoms are shown in Fig. 7. The phantoms are labeled with the corresponding average T_2 values measured by standard 32-echo CPMG MRI (Fig. 7a), and by Dual-τ MRI (Fig. 7b). The T_2 values agree with the CPMG results within 5% up to 70 ms, and 10% up to 100 ms. The consistency check on T_2 measured by CPMG MRI vs SE ^{1}H 1D CSI showed no significant differences (CPMG vs. SE results: 31.1 ± 0.3 vs 31.5 ± 0.3 ms, 38.9 ± 0.5 vs 38.3 ± 1.8 ms, 36.7 ± 0.5 vs 37.5 ± 0.3 ms, 60 ± 6.1 vs 59.4 ± 2.3 ms, 58.6 ± 5 vs 57.7 ± 0.7 ms).

Dual-τ and standard SE T_2 MRI of the foot are compared in Fig. 8. Muscle T_2 values from the Dual-τ image are 29.4 ± 1.2 ms, 28.2 ± 1.6 ms, and 30.6 ± 1.3 ms; as compared to 29.8 ± 2.8 ms, 29.8 ± 4.7 ms, and 28.8 ± 4.7 ms in the same annotated volumes in the CPMG image. These agree with published values for muscle of 32 ± 2 ms at 3 T.[18]. In marrow, CPMG T_2 was 106 ± 4.3 ms as compared to Dual-τ T_2 = 135 ± 13 ms in the same volume, and a prior value of 133 ± 6 ms for marrow[18].

T_2 and T_1 values measured from the Tri-τ experiments on phantoms are compared with SE and PS T_1 and T_2 values in Fig. 9. The values show good agreement for all phantoms.

5. Discussion

Long adiabatic pulses such as BIR-4 are self-refocusing but are subject to T_2 decay, resulting in attenuation by the end of the pulse. We have shown for the first time that T_2 measurements and T_2 image contrast can be obtained using these adiabatic pulse properties as distinct from conventional methods that use spin-echoes or

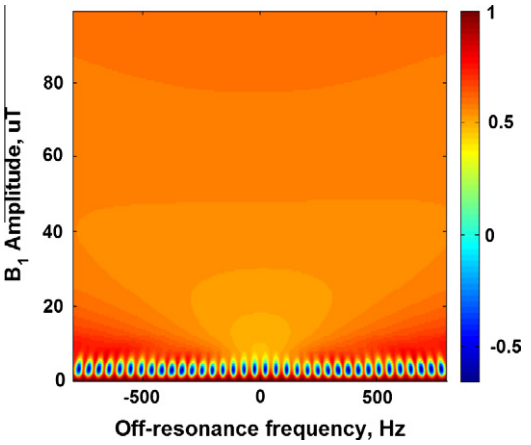

Fig. 5. Contour plot of Mz/Mequ (scale at right) as a function of off-resonance frequency using a 45 ms 0° BIR-4, T_1 = 1115 ms, and T_2 = 55 ms, for comparison with the 45 ms T_2-prep sequence in Ref. [13]. The correct value of Mz/Mequ = exp(−0.81 ∗ 45/T_2) = 0.5 (orange). (For interpretation of the references to colour in this figure legend, the reader is referred to the web version of this article.)

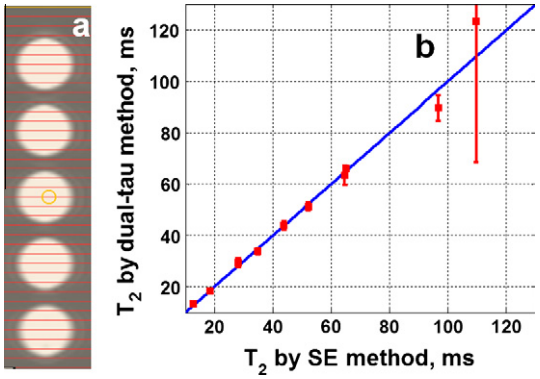

Fig. 6. (a) Transverse image of 5 of the phantoms annotated with 5 mm thick 1DCSI slices (annotated in red). (b) NMR measurements of T_2 from the 10 phantoms using Dual-τ and SE methods. Filled points are the means of the middle three slices of each phantom. Error bars denote ± SD. (For interpretation of the references to colour in this figure legend, the reader is referred to the web version of this article.)

180° refocusing pulses. In particular, we have presented new NMR and MRI pulse sequences for measuring and imaging T_2 that can be performed in just two acquisitions employing long and short duration adiabatic pulses for NMR, or a long and no adiabatic pulse for MRI. These Dual-τ methods were validated for BIR-4 pulses by numerical analysis using the Bloch Equations and experimental ^{1}H NMR and MRI studies of phantoms with different T_2s and MRI of the human foot, compared to conventional SE T_2 measurements (Figs. 3–7). Moreover, extension of the Dual-τ to the Tri-τ method resulted in a technique that not only delivers T_2 measurements but T_1 as well. The Tri-τ method was also validated by both simulations (Fig. 4) and experimental measurements on phantoms (Fig. 9).

Compared to a two-acquisition SE sequence, the efficiency of the Dual-τ method for determining T_2 is the same. Although in principle T_2 could be determined from a single CPMG sequence in half the time of a Dual-τ measurement, the acquisition window for the Dual-τ method is not constrained by the echo spacing and could conceivably benefit from reducing the bandwidth to offset loss in SNR per unit time compared to CPMG. In the Tri-τ method, the T_1-determining portion is based on the Dual-angle T_1 method [12], and hence it has the same efficiency except for the SNR loss due to the T_2 decay that is encoded. The options comparable to the Tri-τ method for obtaining both T_1 and T_2 in three acquisitions are limited and seldom reduced-to-practice. Conceivably, one could use an SE or CPMG sequence to obtain T_2 and a PS [19], SSFP [20] or a Dual-angle [12] sequence to obtain T_1, in which case the total number of acquisitions would be three or more. The Tri-τ method would be comparable or faster than these options.

As with existing techniques for measuring relaxation times, the Dual-τ and Tri-τ methods can be adversely affected by B_1-field nonuniformity when the adiabatic pulses are combined with conventional pulses such as those provided by MRI sequences (Fig. 1). The combined effect of an imperfect slice profile and B_1 inhomogeneity – to which higher-field MRI systems are intrinsically more susceptible – is significant. In order to cancel the denominator in Eq. (1) and obtain a ratio R from which T_2 can be determined using the Dual-τ method, we must have either $\theta = 90°$ or a long TR. Obtaining an exact $\theta = 90°$ slice-selective excitation pulse at 3 T depends on the accuracy of the scanner's set-up routine. Our Dual-τ MRI studies of the foot benefited from the use of a 3D (slab-select) pulse sequence for both the Dual-τ and reference CPMG MRI; selection of just the middle slices; and a longer TR than we would have liked because of errors in the slice-selective 90° pulse. Thus, relative to other T_1 and T_2 methods, the sensitivity of the Dual-τ and Tri-τ methods to B_1 inhomogeneity depends on the pulses

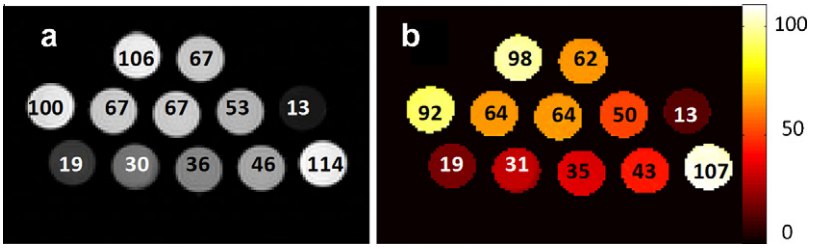

Fig. 7. (a) MRI of the phantom set, T_2-weighted by a 0° 35 ms BIR-4 pre-pulse. The images are annotated with the corresponding reference SE T_2. (b) Color-coded Dual-τ T_2 image with the Dual-τ T_2 values labeled for comparison with part (a).The scale depicts T_2 in ms. The T_2 map is calculated pixel by pixel, and both images masked at the same threshold (=75% of the lowest signal in part a). (For interpretation of the references to colour in this figure legend, the reader is referred to the web version of this article.)

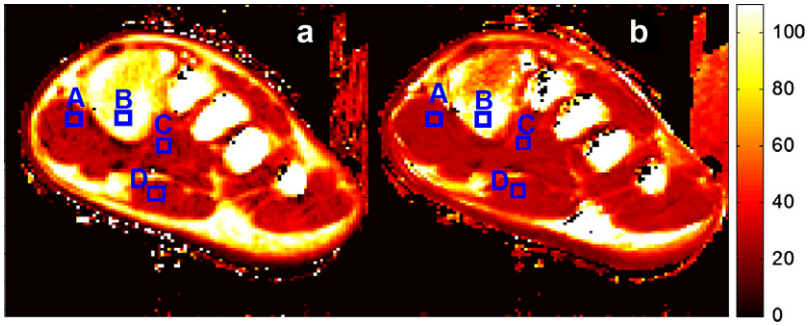

Fig. 8. Coronal T_2 images of the human foot by the SE method (a) and the Dual-τ method (b). The scale depicts T_2 in ms. Both images are calculated pixel-by-pixel and masked by an identical threshold (SNR = 4 in the raw image). Mean T_2s from the annoted squares in (a) vs (b) are: A, 29.8 ± 2.8 ms vs 29.4 ± 1.2 ms; B, 106 ± 4.3 ms vs 135 ± 13 ms; C, 29.8 ± 4.7 ms vs 28.2 ± 1.6 ms; D, 28.8 ± 4.7 ms vs 30.6 ± 1.3 ms.

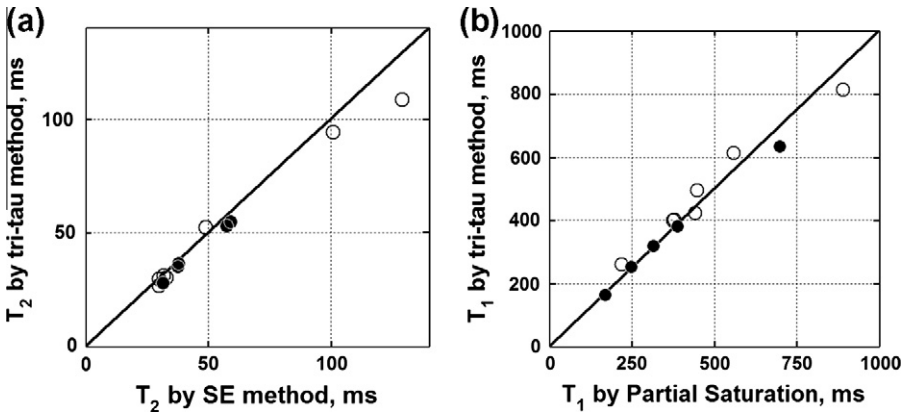

Fig. 9. T_2 and T_1 as measured by a $\tau_3 = 2\tau_2 = 20$ ms Tri-τ experiment from 12 × 1.3 cm ID (empty points) and 4 × 2.5 cm ID (filled points) phantoms, as compared with values measured using standard SE (a) and PS (b) methods (solid line = identity).

being used. Dual-τ errors in T_2 were $\leqslant$7% for up to ±300 Hz frequency offsets, due to the bandwidth of the BIR-4 pulse. However, performing SE T_2 experiments with 35 ms BIR-4 pulses is unrealistic and therefore not directly comparable. All methods employing adiabatic pulses would be expected to exhibit better immunity to B_1 variations than those that do not employ adiabatics.

The delays of several milliseconds added between the 0° BIR-4 pulse, the slice-selective pulse and the echo-times for the MRI sequences, will affect the total attenuation factor, reducing the SNR a little. This did not seem to affect T_2 in the Dual-τ MRI experiment where the delay is the same in both cases. Although the S_1 acquisition of the Tri-τ experiment does not have a delay while the S_2 and S_3 acquisitions do, the Tri-τ T_2 accuracy was also apparently unaffected.

The accuracy of T_1s measured in the Tri-τ NMR experiment will depend critically on the accuracy of the remaining non-adiabatic low-angle (15°) NMR excitation pulses set by the scanner [12]. If MRI is not intended, an adiabatic 15° pulse could avoid this problem provided its duration is $\ll\tau_2$ to avoid a significant 3rd E_{p1} term in Eq (3). Meanwhile, the accuracy of T_1 imaging using a Tri-τ MRI sequence wherein the 60° BIR-4 pulses are replaced by 0° BIR-4 [6] or BIRP [7] pulses, and nominal 60° slice-selective MRI pulses are used for S_2 and S_3 with a 15° slice-selective MRI pulse for S_1, depends on the accuracy with which B_1 and/or the flip-angles are calibrated. Nevertheless, the Tri-τ pulse sequence is presently *unique* in demonstrating a potential for measuring and imaging T_1, T_2 and proton density from just 3 (albeit steady-state) acquisitions – all of which are FIDs.

That the decay in magnetization during the BIR-4 pulse is essentially independent of the flip-angle, enables decoupling of T_2 from the flip-angle, even allowing a T_2 attenuation effect with otherwise zero excitation. In this application, the 0° BIR-4 pulse serves as a T_2

filter, removing the short T_2 components (Fig. 7a), while preserving the longer ones for an FID generated by a subsequent conventional excitation. This could be useful in spectroscopy for removing unwanted short-T_2 components that generate broad baselines. Also, the use of pre-pulses to add T_2 contrast bears similarity to T_2-prep MRI sequences, especially those employing adiabatic pulses [13]. Adiabatic T_2-prep MRI uses several very short 90° AHP and 180° AFP pulses with gaps between them to allow T_2 relaxation [13]. By using a (i) single, (ii) long, (iii) 0° BIR-4 or BIRP pulse, (iv) with no gaps, our sequence differs from that T_2-prep sequence in four ways. Moreover, the present work extends the application from providing T_2 contrast, to providing T_2 measurements.

The use of a single long 0° BIR-4 pulse for T_2-prep instead of the short AHP/AFP pulses [13] may offer some advantage. The long BIR-4 (or BIRP) pulse has a much lower B_1-threshold to achieve adiabaticity than the short AHP, or AFP pulses. As a consequence, it requires much lower peak power. For example, the simulations of a 45 ms AHP/AFP T_2-prep sequence from Fig. 4a of Ref. [13] showed an adiabatic threshold requirement for B_1 of about 20 μT. Performing the same simulation with the same T_1 and T_2 here, showed that a single 45 ms 0° BIR-4 pre-pulse had a B_1 threshold of ~5 μT, or 1/4 that of the AHP/AFP T_2-prep sequence (Fig. 5).

Another question is whether the Dual-τ experiment with long adiabatic pulses measures either the inhomogeneously broadened T_2 (T_2^*) or the T_1 in the rotating frame ($T_{1\rho}$), as distinct from a pure T_2. First, T_2^* results from local B_0-field inhomogeneity or offset frequency, to which a BIR-4 pulse operating above its adiabatic threshold is insensitive over a range of several hundred Hz [12]. In the present studies, both analysis and experiments showed that T_2 varies by $\leqslant$7% for offset frequencies in the range ±300 Hz. Second, $T_{1\rho}$ measures T_1 at the much lower NMR frequency corresponding to the B_1 field. Although it is not explicitly present in the Bloch Equations, $T_{1\rho}$ approaches T_2 as B_1 goes to zero and behaves like a combination of low-frequency T_1 and T_2 [21]. As such, changes in T_1 might be expected to affect Dual-τ T_2 if it were sensitive to $T_{1\rho}$. However, analysis of the Dual-τ experiment showed variations <6% in T_2 over a 5-fold range of T_1 (Fig. 3b). In experiments, Dual-τ T_2 measured at a B_1 of 13.5 μT (knee coil) did not differ by more than 3% from those measured with B_1 = 20 μT (head coil) on the same short- and long-T_2 phantoms. Thus, T_2^* and $T_{1\rho}$ do not appear to be significant factors affecting Dual-τ T_2 measurements in this work.

In conclusion, the Dual-τ method provides a new option for measuring T_2 without requiring any spin echoes, at least for short T_2 tissues such as muscle, cartilage and white matter [22] where the signal ratio affords adequate T_2 resolution (Fig 3a). The same property delivered with an otherwise neutral 0° flip-angle self-refocusing adiabatic pulse can provide T_2-imaging, T_2-weighting, T_2-filtering (Figs. 6 and 7), or T_2-prep (Fig. 9). At the expense of one additional acquisition, the Tri-τ experiment offers the potential for obtaining all of the T_2, T_1 and, because the nuclear density derives directly from the fully-relaxed signal, the proton or signal density information, in just three acquisitions–arguably the minimum possible. The caveat is the requirement for accurate setting and knowledge of the flip-angles. These new methods can potentially save time and simplify relaxation measurements and/or contrast-weighted NMR and MRI.

Acknowledgments

We thank Terri Brawner from the Kennedy Krieger Institute for the loan of a knee coil, and Dr. Refaat E. Gabr, of the Division of MR Research, for helpful discussions and assistance with human studies. The work was supported by NIH Grant R01 EB007829.

References

[1] A. Abragam, The Principles of Nuclear Magnetism, Clarendon Press, Oxford, 1961. p. 599.
[2] D.G. Norris, Adiabatic radiofrequency pulse forms in biomedical nuclear magnetic resonance, Concepts Magn. Reson. 14 (2002) 89–101.
[3] R.A. De Graaf, K. Nicolay, Adiabatic rf pulses: applications to in vivo NMR, Concepts Magn. Reson. 9 (1997) 247–268.
[4] M.S. Silver, R.I. Joseph, D.I. Hoult, Highly selective [pi]/2 and [pi] pulse generation, J. Magn. Reson. 59 (1984) 347–351.
[5] C.J. Hardy, W.A. Edelstein, D. Vatis, Efficient adiabatic fast passage for NMR population inversion in the presence of radiofrequency field inhomogeneity and frequency offsets, J. Magn. Reson. 66 (1986) 470–482.
[6] M. Garwood, Y. Ke, Symmetric pulses to induce arbitrary flip angles with compensation for rf inhomogeneity and resonance offsets, J. Magn. Reson. 94 (1991) 511–525.
[7] P.A. Bottomley, R. Ouwerkerk, BIRP: an improved implementation of low-angle adiabatic (BIR-4) excitation pulses, J. Magn. Reson., Ser. A 103 (1993) 242–244.
[8] M. Robin Bendall, M. Garwood, K. Uğurbil, D.T. Pegg, Adiabatic refocusing pulse which compensates for variable of power and off-resonance effects, Magn. Reson. Med. 4 (1987) 493–499.
[9] A.-M. El-Sharkawy, M. Schar, R. Ouwerkerk, R.G. Weiss, P.A. Bottomley, Quantitative Cardiac ^{31}P spectroscopy at 3 Tesla using adiabatic pulses, Magn. Reson. Med. 61 (2009) 785–795.
[10] S. Meiboom, D. Gill, Modified spin-echo method for measuring nuclear relaxation times, Rev. Sci. Instrum. 29 (1958) 688–691.
[11] P.A. Bottomley, W.A. Edelstein, NMR Imaging of the Transverse Relaxation Time Using Multiple Spin Echo Sequences. US Patent 4521,733 (June 4, 1985).
[12] P.A. Bottomley, R. Ouwerkerk, The dual-angle method for fast, sensitive T_1 measurement in vivo with low-angle adiabatic pulses, J. Magn. Reson. B 104 (1994) 159–167.
[13] R. Nezafat, R. Ouwerkerk, A.J. Derbyshire, M. Stuber, E.R. McVeigh, Spectrally selective B_1-insensitive T_2 magnetization preparation sequence, Magn. Reson. Med. 61 (2009) 1326–1335.
[14] P.A. Bottomley, W.A. Edelstein, Method of Eliminating Effects of Spurious Free Induction Decay NMR Signal caused by Imperfect 180 Degrees Pulses. US Patent 4484,138 (November 20, 1984).
[15] J. Bittoun, J. Taquin, M. Sauzade, A computer algorithm for the simulation of any nuclear magnetic resonance (NMR) imaging method, Magn. Reson. Imaging 2 (1984) 113–120.
[16] K. Yoshimura, H. Kato, M. Kuroda, A. Yoshida, K. Hanamoto, A. Tanaka, M. Tsunoda, S. Kanazawa, K. Shibuya, S. Kawasaki, Y. Hiraki, Development of a tissue-equivalent MRI phantom using carrageenan gel, Magn. Reson. Med. 50 (2003) 1011–1017.
[17] A. Naressi, C. Couturier, J.M. Devos, M. Janssen, C. Mangeat, R.d. Beer, D. Graveron-Demilly, Java-based graphical user interface for the MRUI quantitation package, MAGMA 12 (2001) 141–152.
[18] G.E. Gold, E. Han, J. Stainsby, G. Wright, J. Brittain, C. Beaulieu, Musculoskeletal MRI at 3.0 T: relaxation times and image contrast, Am. J. Roentgenol. 183 (2004) 343–351.
[19] X. Liu, Y. Feng, Z.-R. Lu, G. Morrell, E.-K. Jeong, Rapid simultaneous acquisition of T_1 and T_2 mapping images using multishot double spin-echo EPI and automated variations of TR and TE (ms-DSEPI-T12), NMR Biomed. 23 (2010) 97–104.
[20] S.C.L. Deoni, B.K. Rutt, T.M. Peters, Rapid combined T_1 and T_2 mapping using gradient recalled acquisition in the steady state, Magn. Reson. Med. 49 (2003) 515–526.
[21] P.R. Moran, C.A. Hamilton, Near-resonance spin-lock contrast, Magn. Reson. Imaging 13 (1995) 837–846.
[22] N. Gelman, J.M. Gorell, P.B. Barker, R.M. Savage, E.M. Spickler, J.P. Windham, R.A. Knight, MR imaging of human brain at 3.0 T: preliminary report on transverse relaxation rates and relation to estimated iron content, Radiology 210 (1999) 759–767.